Impacts of El Niño and La Niña on the U.S. Climate during Northern Summer

ZHUO WANG AND C.-P. CHANG

Department of Meteorology, Naval Postgraduate School, Monterey, California

BIN WANG

Department of Meteorology, University of Hawaii at Manoa, Honolulu, Hawaii

(Manuscript received 20 May 2005, in final form 11 September 2006)

ABSTRACT

The impacts of El Niño and La Niña on the U.S. climate during northern summer are analyzed separately. Composite analyses reveal that a continental-scale anomalous high dominates over most of North America during La Niña events and leads to hot and dry summers over the central United States. However, the impacts of El Niño over North America are weaker and more variable.

A linear barotropic model is used to explore the maintenance of the anomalous patterns. Various forcing terms derived from observations via a single-level vorticity budget analysis are used to drive the model. When the barotropic model is driven by the total forcing (Rossby wave source plus transient eddy forcing plus nonlinear interactions), the model simulations resemble the observed patterns, and a strong and extensive anticyclone is reproduced in the La Niña simulation. The model responses to the individual forcing terms suggested that the vorticity stretching term (fD) and the transient eddy forcing contribute most to the responses over North America. The stretching term (fD) excites a low in the El Niño simulation and a high in the La Niña simulation over North America. However, the transient eddy forcing favors an anomalous high over North America in both El Niño and La Niña simulations, such that it weakens the El Niño pattern and strengthens the La Niña pattern.

1. Introduction

How the El Niño–Southern Oscillation (ENSO) impacts the North American climate during boreal summer has been explored in many previous studies but remains a controversial topic. For instance, Namias (1991) found that the composite 700-hPa geopotential height pattern during La Niña events has small perturbations over North America, and Adams and Comrie (1997) concluded that the interannual variability of the North America monsoon (NAM) is not strongly linked to El Niño. On the other hand, Trenberth and collaborators suggested that the severe 1988 North American summer drought was related to the La Niña event (Trenberth et al. 1988; Trenberth and Branstator 1992; Trenberth and Guillemot 1996). Ting and Wang (1997) found that the summer rainfall in the central United States has a good correlation with the SST anomalies (SSTA) associated with El Niño using 1950–90 data. However, Ropelewski and Halpert (1986) found no consistent relationship between the U.S. summer rainfall variability and ENSO in a dataset covering a different period (1875–1980).

In most of the aforementioned studies, correlation or regression analyses were used as the primary tool to diagnose the relationship between ENSO and the U.S. rainfall anomalies. The underlying premise for correlation or regression analysis is that the response to ENSO is linear. That is, the anomalies in the El Niño phase are nearly an inverse of those in the La Niña phase. This assumption has been questioned by some studies. Halpert and Ropelewski (1992) examined the large-scale temperature anomalies associated with the low and high phases of the Southern Oscillation and found asymmetric impacts in some regions. Montroy et al. (1998) showed some nonlinear characteristics of the observed teleconnections between the tropical Pacific SSTAs and the central and eastern North American precipitation. Hoerling et al. (1997, 2001) found that during Northern winter the La Niña pattern shifts westward with the high SSTs and is nearly in quadra-

Corresponding author address: Dr. Zhuo Wang, Department of Meteorology, Naval Postgraduate School, Monterey, CA 93943.
E-mail: zwang@nps.edu

DOI: 10.1175/JCLI4118.1

ture with the El Niño pattern over the North Pacific and North America. Wu and Hsieh (2004) found that the 500-hPa geopotential height perturbations have a good correlation with the square of the SSTAs in the east Pacific in Northern winter.

The asymmetry or nonlinearity of the atmospheric response to SST anomalies in Northern winter is also found in some AGCM simulations. Geisler et al. (1985) found that the amplitude of the AGCM response in the midlatitudes is insensitive to the increase in the tropical precipitation anomaly beyond a certain value. Pitcher et al. (1988) and Kushnir and Lau (1992) found that the Pacific–North America (PNA) pattern of the same polarity may be excited by the warm and cold SSTAs in the North Pacific and that the response to a cold SSTA is *stronger and more coherent*. Through analysis of observations and a large ensemble of AGCM simulations, Sardeshmukh et al. (2000) examined the changes of the probability distributions of atmospheric variables associated with ENSO events and found a substantial asymmetry in remote responses to El Niño and La Niña. Hoerling et al. (2001) attributed the nonlinearity of the ENSO teleconnection to the intrinsic nonlinear relationship between tropical SSTAs and deep convection. Kushnir and Lau (1992) diagnosed the baroclinic eddies in the AGCM simulations and suggested that baroclinic eddies play an important role in determining the extratropical atmospheric response to SST anomalies. Other possible sources of nonlinearity include the nonlinear topographic effects and nonlinear wave–wave interactions. The former play a role in maintaining the extratropical low-frequency patterns (Hoerling and Ting 1994; Ting et al. 1996, 2001; Ting and Yu 1998), and the latter modify the structure and location of the atmospheric response (Kang and Held 1986; Hall and Derome 2000).

In this study, we examine the impacts of ENSO on the U.S. climate during Northern summer. The El Niño and La Niña events are investigated separately to reveal some important information that was not shown by previous linear analyses. The datasets and the model used in this study are briefly described in section 2. Section 3 presents the results of the observational analyses. Barotropic model simulations are discussed in section 4. A brief summary and discussion follows in section 5.

2. Datasets, analysis methods, and models

a. Data

The Niño-3 time series derived from the extended reconstructed sea surface temperature (ERSST) dataset (Smith and Reynolds 2004) during 1901–2004 are used to identify El Niño and La Niña events. The ERSST dataset was constructed using the most recently available SST data from the Comprehensive Ocean–Atmosphere Data Set (COADS) and improved statistical methods that allow stable reconstruction using sparse data. It also uses sea ice concentrations to improve the high-latitude SST analysis and includes an improved error estimate.

Besides ERSST, several other datasets are used for the composite analyses. The National Centers for Environmental Prediction–National Center for Atmospheric Research (NCEP–NCAR) reanalysis has a $2.5° \times 2.5°$ spatial resolution and covers the period from 1948 to the present (Kalnay et al. 1996). The University of Delaware precipitation and surface air temperature (UDel_AirT_Precip) dataset, which is derived from station data, covers the global land area at a $0.5° \times 0.5°$ resolution and is available during 1950–99. Precipitation and surface air temperature data from the Climate Research Unit (CRU TS 2.0) are also used, which is available for a longer time period (1901–2002) and covers the global land surface at a $0.5° \times 0.5°$ resolution.

The impacts of El Niño and La Niña on interannual time scales are the focus of this study. Prior to the composite analyses, an 11-yr running mean high-pass filter was applied to both the Niño-3 time series and the time series of the analyzed fields to remove decadal signals. At the beginning and the end of the time series, the closest possible approximation to the low-frequency signals is used (e.g., the average during 1994–2004 is used for 2004). It is well known that ENSO is phased locked to the annual cycle. It usually begins in Northern spring or summer, matures in Northern winter, and decays in the following spring. Warm and cool summers in the ENSO developing phase are examined in this study. El Niño (La Niña) years are selected if both the summer and the following winter Niño-3 SST anomalies are positive (negative) and exceed the corresponding 0.9 standard deviation (the standard deviation of the Niño-3 SST index is about 0.75 K in summer and 1.0 K in winter). The years selected for composites are listed in Table 1. The ENSO events during 1950–95 are a subset of the ENSO events defined by Trenberth (1997), who used a lower criterion (0.4 K). The response to El Niño/La Niña is defined as the difference between the sample mean of El Niño/La Niña events and the climatological mean based on all the years during the period of interest. Two sample Student's t tests are used to check the significance of the composites.

TABLE 1. Warm and cold summers for composite analyses during 1948–2004 and 1901–2002, respectively. Niño-3 SSTA during summer and the following winter both exceed 0.9 of the corresponding standard derivation threshold. The 11-yr running means are removed from the Niño-3 time series.

	1948–2004	1901–2002
El Niño	1957, 1965, 1972, 1976, 1982, 1991, 1997	1902, 1905, 1918, 1930, 1939, 1941, 1951, 1957, 1965, 1972, 1976, 1982, 1991, 1997
La Niña	1955, 1970, 1973, 1975, 1988, 1999	1903, 1909, 1910, 1916, 1924, 1942, 1955, 1970, 1973, 1975, 1988, 1999

b. Barotropic model and vorticity budget analysis

A linear nondivergent barotropic model is used to diagnose the maintenance of the extratropical response. The barotropic model can be written as

$$\frac{\partial \zeta_a}{\partial t} + \mathbf{V}_{\psi c} \cdot \nabla \zeta_a + \mathbf{V}_{\psi a} \cdot \nabla(\zeta_c + f) = S - (\gamma + K\nabla^4)\zeta_a, \tag{1}$$

where $()_c$ denotes the climatological mean, $()_a$ denotes the seasonal mean anomalies, S is the vorticity forcing, and γ is a drag coefficient equal to $(15\ \text{day})^{-1}$. The diffusion coefficient K is specified so that the e-folding time scale for the smallest-scale eddies resolved in the model is 1 day. The basic state used in the model is the 200-hPa summer climatological mean streamfunction derived from the NCEP–NCAR reanalysis. The steady-state response of the model with a T42 spatial resolution is solved by matrix inversion.

Various forcing terms derived from observations via a single-level vorticity budget analysis are used to drive the model. The equation for the vorticity budget analysis may be written as

$$\frac{\partial \zeta_a}{\partial t} + \mathbf{V}_{\psi,c} \cdot \nabla \zeta_a + \mathbf{V}_{\psi,a} \cdot \nabla(\zeta_c + f) = \underbrace{-\nabla \cdot [\mathbf{V}_{\chi,c}\zeta_a + \mathbf{V}_{\chi,a}(\zeta_c + f)]}_{\text{RWS}} \underbrace{-\nabla \cdot \overline{(\mathbf{V}'\zeta')}_a}_{\text{Eddy}} \underbrace{-\nabla \cdot \overline{(\mathbf{V}_{\psi,a}\zeta_a)}_a}_{\text{Nlin}} + R, \tag{2}$$

where $()'$ denotes transient eddies, $\overline{(\ldots)}$ denotes a sample mean, the subscripts ψ and χ represent the rotational and divergent components of the wind field, respectively, and R is the residual term. The first term on the right-hand side of Eq. (2) is usually considered a Rossby wave source (RWS), which includes vorticity advection by the divergent flow and the stretch ing terms. The next term is the anomalous transient eddy forcing, which is derived from daily mean data. The third term on the right-hand side of Eq. (2) is the nonlinear advection by the rotational wind. The residual term may include damping, subgrid, and other unresolved processes. For a low-frequency pattern represented by monthly or seasonal mean anomalies, the time tendency on the left-hand side of Eq. (2) may be taken as zero.

The Rossby wave source is associated with divergent flows and may be further decomposed into the following terms:

$$\text{RWS} = \underbrace{-\beta v_{\chi,a}}_{\text{RWS1}} \underbrace{-\mathbf{V}_{\chi,a} \cdot \nabla \zeta_c}_{\text{RWS2}} \underbrace{-\mathbf{V}_{\chi,c} \cdot \nabla \zeta_a}_{\text{RWS3}} \underbrace{-f\nabla \cdot \mathbf{V}_{\chi,a}}_{\text{RWS4}} \underbrace{-\zeta_c \nabla \cdot \mathbf{V}_{\chi,a}}_{\text{RWS5}} \underbrace{-\zeta_a \nabla \cdot \mathbf{V}_{\chi,c}}_{\text{RWS6}}. \tag{3}$$

The terms on the right-hand side are the β effect (RWS1—the planetary vorticity advection by the anomalous divergent flow), advection of the mean relative vorticity by the anomalous divergent flow (RWS2), advection of the anomalous vorticity by the mean divergent flow (RWS3), the stretching effect due to anomalous divergence (RWS4 and RWS5), and the stretching effect due to mean divergence (RWS6).

3. Extratropical responses to El Niño and La Niña

Composites of 500-hPa height and SST for El Niño and La Niña events during 1948–2004 are shown in Fig.

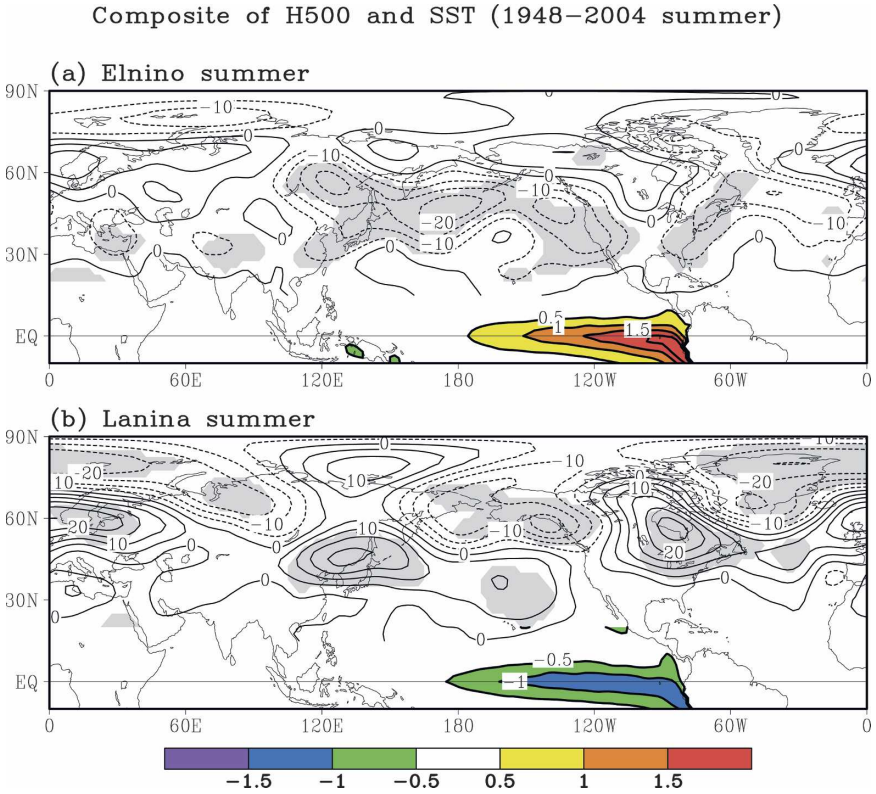

FIG. 1. Composites of 500-hPa height (15°–90°N) and tropical SSTAs (color shading; K) for (a) El Niño and (b) La Niña events during 1948–2004. Gray shading indicates height anomalies above the 95% confidence level. SSTAs below the 95% confidence level are not shown.

1. The warm SST anomalies in the El Niño composite (Fig. 1a) are generally stronger than the cold SST anomalies (Fig. 1b) in the La Niña composite, with a maximum above 2 K south of the equator near the coast of Peru. In the El Niño composite, an elongated anomalous low extends from East Asia to the west coast of North America between 30° and 60°N, and it corresponds to a strengthened jet stream over East Asia and the North Pacific. Another anomalous low is found over the east coast of North America and the midlatitude North Atlantic. A weak (below 95% confidence level) high covers North America. In the La Niña composite (Fig. 1b), an anomalous high extends from East Asia southeastward to the mid-North Pacific. Over East Asia, the La Niña pattern is opposite to the El Niño pattern, which suggests a linear relationship between the eastern Pacific SSTAs and precipitation anomalies over east Asia. To the north of the anomalous high, a low extends along the northern rim of the Pacific Ocean. A high is dominant over North America and extends eastward to Europe, with a low to its north. Overall, the extratropical responses to El Niño and La Niña exhibit different spatial patterns. Although the eastern Pacific SSTAs are stronger in the El Niño composite than in the La Niña composite, the geopotential height response to La Niña is stronger over North America, the North Atlantic, and Europe. An examination of the response in the individual years reveals that the response to La Niña is robust in that it resembles the composite mean in most La Niña years. However, the response to El Niño is more variable.

The vertical structure of the patterns is demonstrated by the composites of 200- and 700-hPa wind fields in Fig. 2 and Fig. 3, respectively. The extratropical response has an equivalent barotropic vertical structure, and all of the circulation anomalies mentioned above are present at both 200 and 700 hPa, with the low-level response weaker than the upper-level response. Over south Asia, the upper-level westerly anomalies in the El Niño composite and easterly anomalies in the La Niña composite suggest an inverse relationship between the Indian summer monsoon and ENSO (e.g., Webster and Palmer 1997). In the El Niño composite, a pair of upper-level anticyclones is found over the central and western tropical Pacific, with an anomalous easterly flow along the equator (Fig. 2), which resembles the Matsuno–Gill (Matsuno 1966; Gill 1980) pattern. A pair of cyclones is present in the lower troposphere

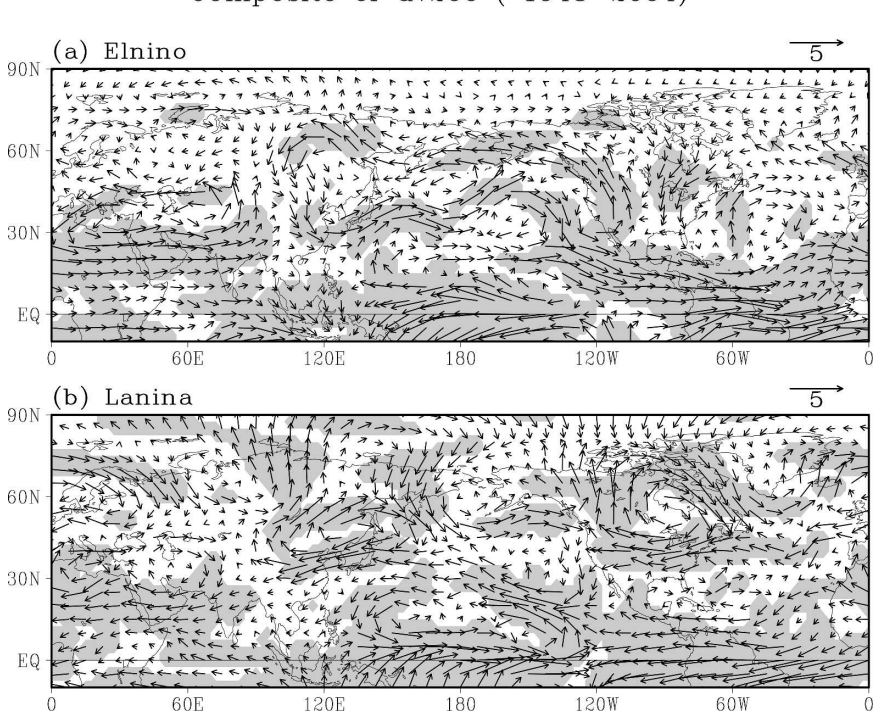

FIG. 2. Composites of 200-hPa wind field for (a) El Niño and (b) La Niña events during 1948–2004. Gray shading indicates height anomalies above the 95% confidence level.

(Fig. 3), which suggests a baroclinic vertical structure in the Tropics. The tropical response to La Niña has a similar pattern with opposite signs, which is different from the asymmetry shown in the extratropical responses.

The composites of surface air temperature and precipitation over North America during 1950–99 are shown in Fig. 4. For El Niño, cold anomalies are found over the southern and eastern United States; for La Niña, the temperature anomalies are colder over the west coast of Canada and warmer over the northeastern central United States and central Canada. Consistent with the circulation anomalies, the impacts of La Niña on surface temperature are stronger and coherent. Figures 4c,d show that rainfall is mostly reduced in the east and enhanced in the west during El Niño events, while in the La Niña composite, rainfall is deficient over the United States and excessive north of 60°N. This is consistent with Mo et al. (1997), who found that the central U.S. drought may be traced back to the eastern Pacific while the wave train associated with the central U.S. flood originated from the western North Pacific.

Some studies (DeWeaver and Nigam 2002; Hu and Feng 2001; Hu 2003) found that decadal changes in the North Pacific SST may modulate the ENSO teleconnections. DeWeaver and Nigam (2002) suggested that the nonlinearity found by Hoerling et al. (2001) was due to the decadal variations related to the phase change of the North Pacific Oscillation (NPO) in the 1970s, because the composite cases in Hoerling et al.'s study were not evenly distributed in the NPO high and low phases. Gershunov and Barnett (1998) found that El Niño patterns are strong and consistent only during the high phases of the North Pacific Oscillation in Northern winter and La Niña patterns are strong and consistent during the low phases of NPO. Although an 11-yr running mean filter was applied to all time series prior to composite analyses, aperiodic decadal signals may still exist. To see if the stronger La Niña pattern is due to the modulation by NPO, the composites of 500-hPa geopotential height were constructed for 1948–78, which is usually regarded as a low phase of NPO or a cold phase of the Pacific decadal oscillation (PDO). The El Niño pattern over the North Pacific (Fig. 5a) is similar to that in Fig. 1a, with a ridge across North America. The La Niña pattern (Fig. 5b) resembles the composite pattern during 1948–2004 (Fig. 1b) and the anomalous high over North America is even stronger. We also examined the composites during an NPO high phase, 1979–99 (not shown). The La Niña pattern is similar to those during 1948–2004 and 1948–78 over the North Pacific and North America, but the El Niño pat-

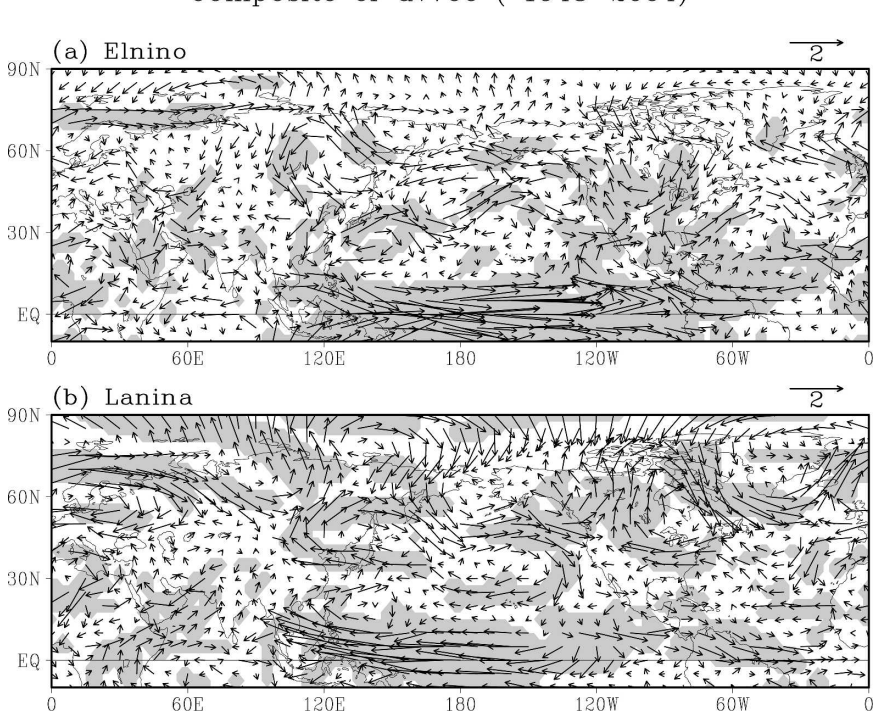

FIG. 3. Same as Fig. 2, but for 700-hPa wind field.

tern has more differences. It is not clear whether this reflects a decadal change or is due to the small sample size (1979–99).

To test the robustness of the results, we also analyzed the 1901–2002 CRU TS 2.0 dataset, which doubles the sample size (Table 1). Composites of surface temperature and precipitation over North America are shown in Fig. 6. Although the magnitudes of the anomalies are smaller, the anomaly patterns of both variables are similar to those in Fig. 4. Because the signals are weak for the first half of the century, the composites are dominated by the recent 52 yr, which are very similar to those produced from the University of Delaware data. This result is consistent with Hu and Feng (2001), who found that the impacts of ENSO on the U.S. summer climate have decadal variations and were weak during 1917–49.

4. Simple barotropic model simulation

It is intriguing that compared to El Niño, the somewhat weaker SSTAs during the La Niña events are associated with a stronger response over North America. A linear barotropic model is used in this section to diagnose the maintenance of the extratropical responses to El Niño and La Niña forcings and especially why the La Niña pattern over North America is stronger than the El Niño pattern. The one-level vorticity budgets are derived using Eq. (2) with the NCEP–NCAR 200-hPa wind fields for the period 1948–2004. Rotational and divergent winds are derived from the streamfunction and velocity potential, respectively. The selected El Niño and La Niña cases are the same as those shown in Table 1. In this analysis, an 11-yr running mean filter was not applied to the wind field data.

In the Tropics, diabatic heating is approximately balanced by adiabatic cooling, and thus the divergence anomaly is linked to thermal forcing. In the extratropical regions, the divergence anomaly may be a manifestation of the remote response. On the other hand, high-frequency eddy feedback and nonlinear advection in the midlatitudes may play an important role in determining the extratropical perturbations (Kang and Held 1986; Held et al. 1989, 2002; Hoerling and Ting 1994), and they should be regarded as part of the forcing. Therefore, the barotropic model forcing function was calculated from the observational data by including the Rossby wave source term in Eq. (2) between 30°S and 30°N and the nonlinear term and the eddy term between 80°S and 80°N (forcing in higher latitudes contains large errors).

For comparison, the composites of the 200-hPa streamfunction for El Niño and La Niña events during 1948–2004 are shown in Figs. 7a,b. Zonal means are removed to better illustrate the wavelike structure. Al-

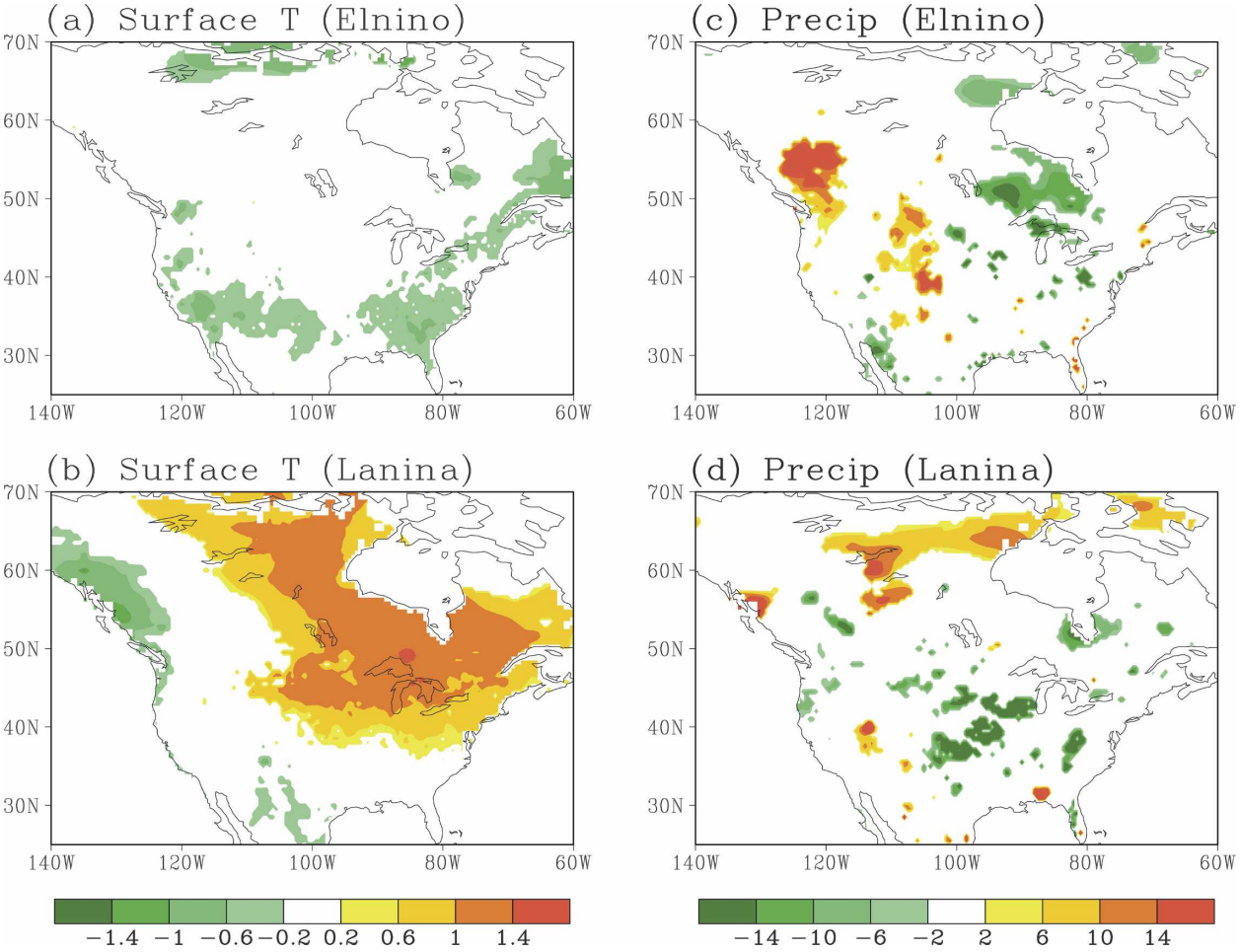

FIG. 4. Composites of (a), (b) surface air temperature (K) and (c), (d) precipitation (mm month^{-1}) anomalies over North America from UDel datasets during 1950–99 for El Niño and La Niña events. Here (a), (c) are the El Niño composites and (b), (d) are the La Niña composites. Only differences above the 95% confidence level are shown.

though unfiltered streamfunction data are used to construct the composites in Figs. 7a,b, the patterns resemble the 200-hPa wind composites (Fig. 2). While the El Niño pattern has a three-cell wave train structure from the equatorial Pacific to North America, the La Niña composite has a four-cell wave train pattern. Both patterns have an anticyclone over North America and the La Niña response is stronger. Although one might expect that the different spatial structures of the El Niño and La Niña patterns over the North Pacific and North America might be due to the different mean states in El Niño and La Niña events, the barotropic model simulations suggest that the response is not sensitive to the subtle changes in the mean flow (not shown).

The barotropic model-simulated El Niño and La Niña patterns when the Rossby wave source, eddy forcing, and nonlinear terms are all included are shown in Figs. 7c,d. The model simulations capture certain key features of the observed anomalies. For example, the anticyclone over North America and the cyclone over the western and central North Pacific in the La Niña composite are simulated in the model. Similar to the observations, the model's El Niño response and La Niña response both have an anticyclone over North America, and the La Niña anticyclone is stronger and more extensive.

Table 2 contains the spatial correlation between the observed patterns and the model simulations over the region of interest (0°–75°N, 90°E–360°E). The model-simulated El Niño pattern is positively correlated with the observed El Niño pattern at 0.59, while it is negatively correlated with the observed La Niña pattern at −0.60. This significant and out-of-phase contrast is similarly present in the model-simulated La Niña pattern (correlation of −0.48 with observed El Niño and

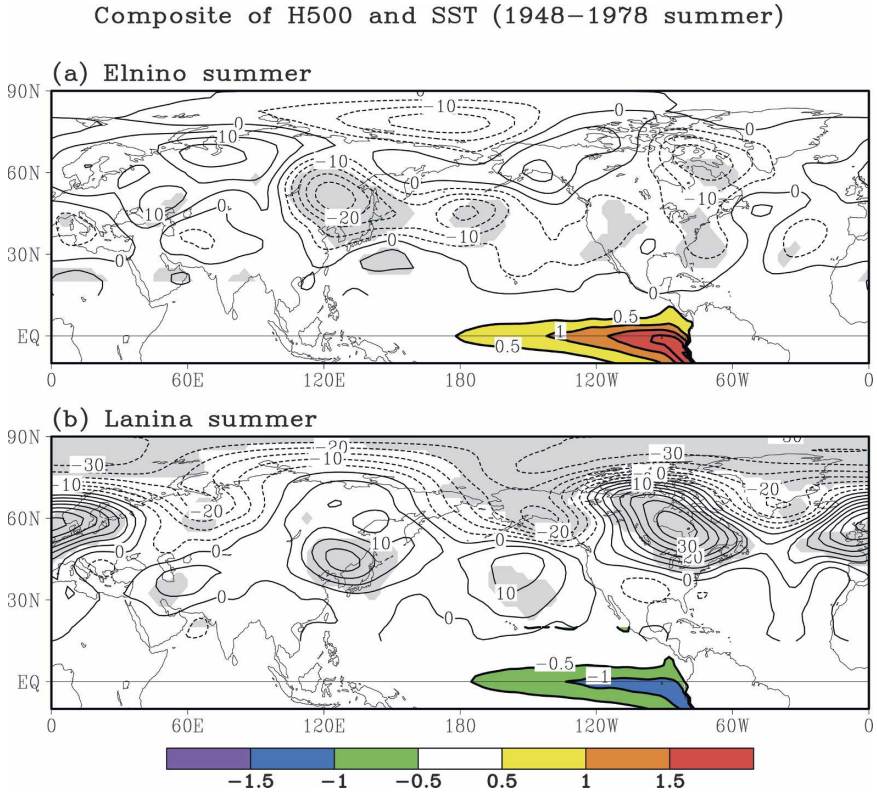

FIG. 5. Same as Fig. 1, but for the period 1948–78.

+0.58 with observed La Niña). An even higher correlation (+0.73) exists between the model-simulated El Niño–La Niña pattern difference and the observed difference. These consistent correlations indicate that the observed El Niño and La Niña patterns are substantially represented in the barotropic model simulations.

The major discrepancy between the simulations and the observations is the westward and equatorward shift of the model simulation compared to the observation, which may be due to the omission of complete nonlinearity in the barotropic model. Previous studies (e.g., Kang and Held 1986; Hall and Derome 2000) suggested that nonlinearity may change the position of the response. In particular, Hall and Derome (2000) showed that nonlinear wave–wave interactions cause the response to El Niño to shift eastward over the North Pacific.

We examined the barotropic model responses to individual forcing terms and found that the β-term (the planetary vorticity advection by the anomalous divergent flow), the stretching term (fD), and the eddy term are most important. The nonlinear term generates El Niño and La Niña responses of the same polarity and enhances the asymmetry of the El Niño and La Niña responses. The residual forcing mainly acts as a damping term.

The barotropic model responses to the sum of the three dominant forcing terms ($\beta v_\chi + fD$ + eddy) are shown in Figs. 8a,b. They capture the key features of the responses to the total forcing (Figs. 7c,d). The model responses to the three individual forcing terms are shown in Figs. 8c–h. The strong response to the β-term is mainly confined in the Tropics, and the La Niña response is almost a mirror image to the El Niño response (Figs. 8c,d). The stretching term excites responses in both tropical and extratropical regions (Figs. 8e,f). Over North America, it generates a cyclone in the El Niño simulation and an anticyclone in the La Niña simulation, and the anticyclone is stronger.

The transient eddy forcing produces rather asymmetric responses (Figs. 8g,h). It generates an anticyclone over North America in both El Niño and La Niña simulations. The transient eddy forcing thus enhances the response to the stretching term in the La Niña simulation and contributes to a strong anticyclone over North America. In the El Niño case, it cancels the response to the stretching term and leads to a weak anticyclone over North America.

Further simulations show that the forcings in the Southern Hemisphere excite very weak responses in the Northern Hemisphere and can be neglected. We now focus on the Northern Hemisphere, and decom-

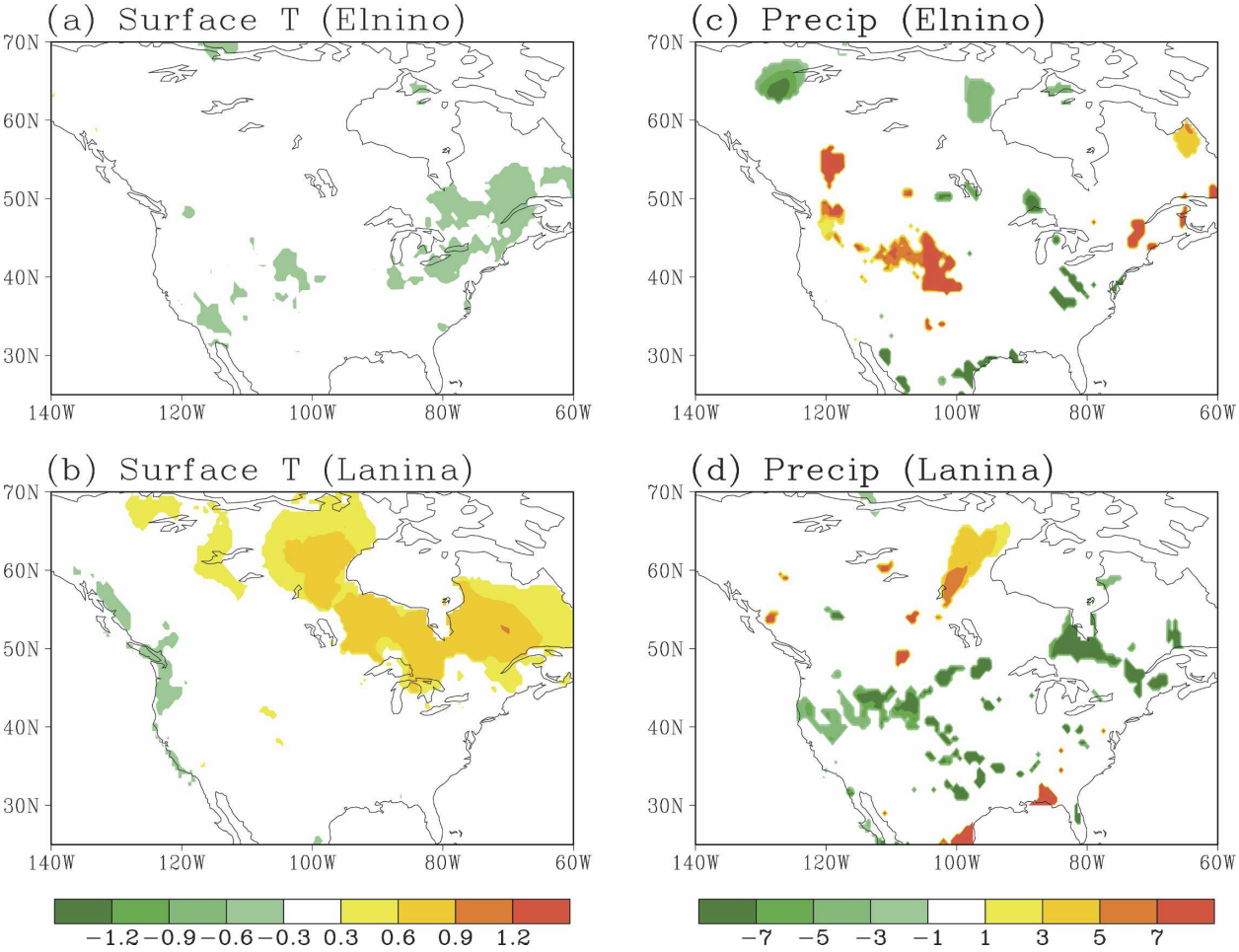

FIG. 6. Same as Fig. 4, but for the period 1901–2002 (derived from CRU dataset).

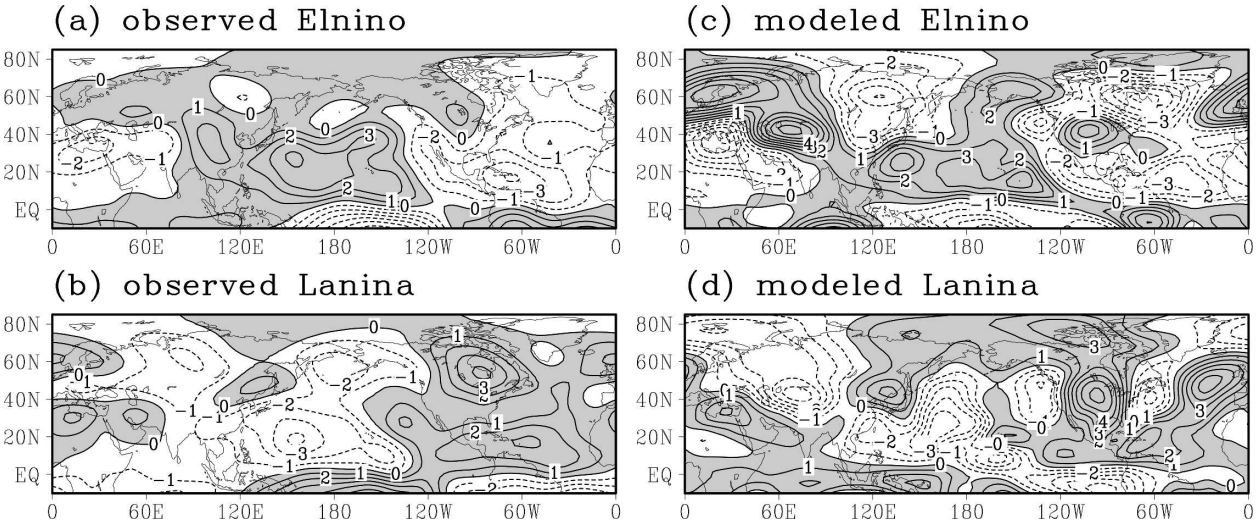

FIG. 7. Composites of 200-hPa streamfunction (10^6 m^2 s^{-1}) for (a) El Niño and (b) La Niña years during 1950–2004 derived from the NCEP–NCAR reanalysis. Barotropic model-simulated (c) El Niño and (d) La Niña patterns. The gray shading in (a), (b) indicates negative values. Zonal mean components are removed in (a)–(d).

TABLE 2. Spatial correlations between the modeled and observed El Niño and La Niña patterns over (0°–75°N, 90°–360°E).

Spatial correlation	Observed El Niño	Observed La Niña
Model El Niño	0.59	−0.60
Model La Niña	−0.48	0.58

pose the stretching term and the eddy term in different regions to trace the origin of the extratropical response. In the model simulations in Figs. 9a,b, the stretching forcing was derived from the vorticity budget analysis in the region (0°–30°N, 0°–180°E) and was set as zero outside this region. The model responses to stretching forcing over (0°–30°N, 0°–180°W) are shown in Figs. 9c,d. When the forcing is confined to the Eastern Hemisphere (Figs. 9a,b), a wave train emanates from the Mediterranean region and extends along a great circle route to reach North America. Wang et al. (2005) suggested that the southerly mean flow associated with the south Asian summer anticyclone may transfer Rossby wave sources northward and excite an extratropical wave train. The wave train generates an anticyclone over northern North America and a cyclone over south-

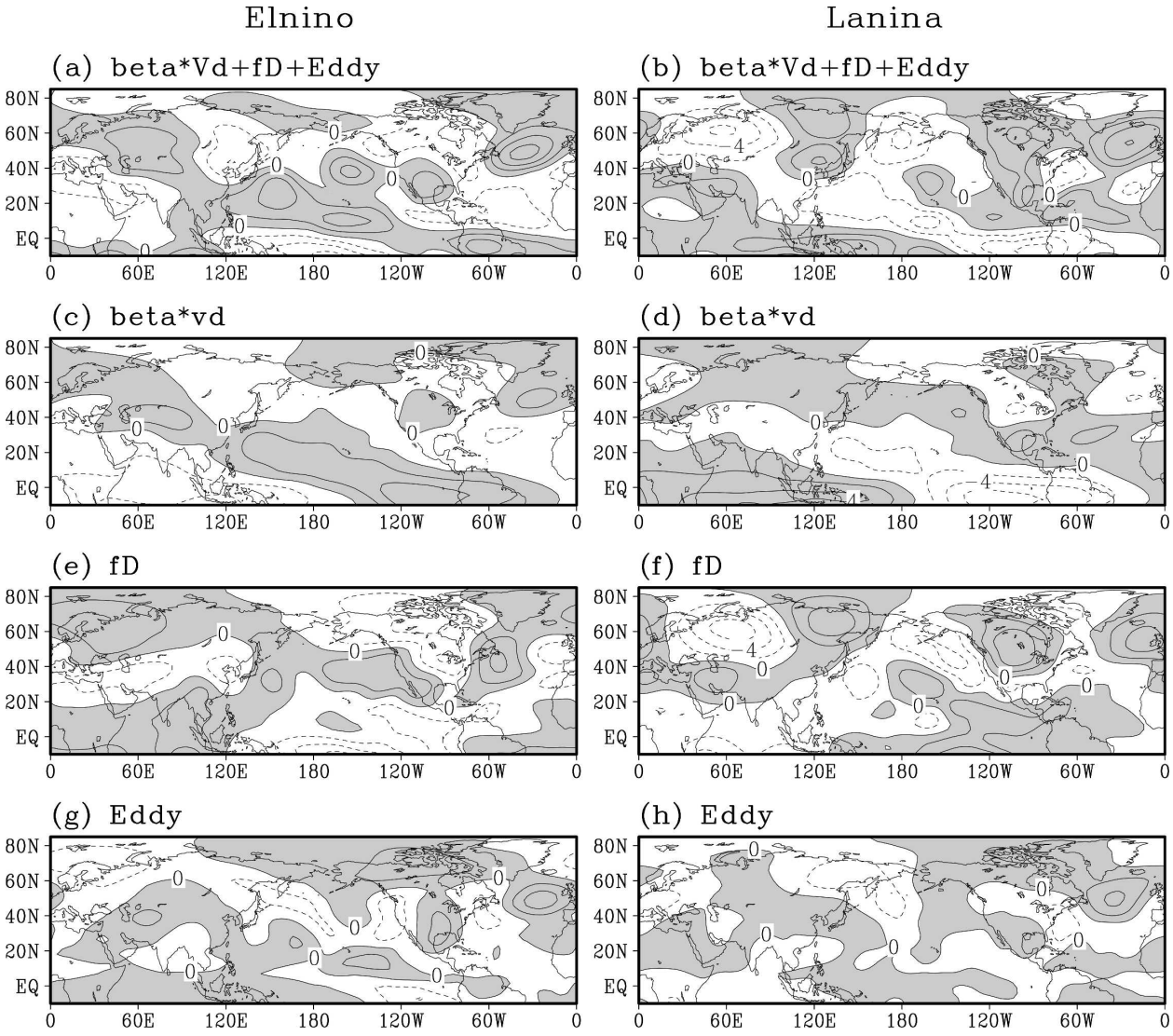

FIG. 8. The steady responses of the barotropic model to various forcing terms as derived from the vorticity budget (10^6 m^2 s^{-1}): (a), (b) the sum of the beta term, the stretching term, and the eddy term; (c), (d) the beta term; (e), (f) the stretching term; and (g), (h) the eddy term. The El Niño response is shown in (a), (c), (e), (g) and the La Niña response in (b), (d), (f), (h). The gray shading indicates positive values. The zonal mean components are removed.

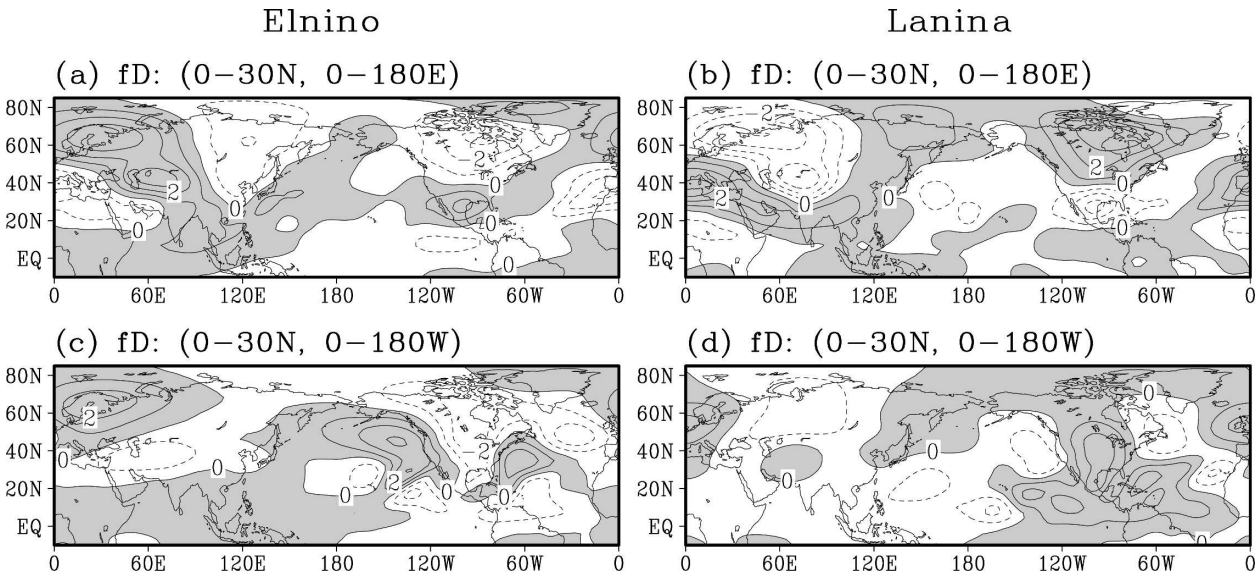

FIG. 9. Barotropic model responses to the stretching term, *fD*, in different regions: (a), (b) 0°–30°N, 0°–180°E and (c), (d) 0°–30°N, 180°W–0°.

ern North America in the La Niña case. The El Niño response is opposite to the La Niña response and is slightly weaker. The stretching forcing over only the Western Hemisphere (0°–30°N, 0°–180°W) excites a wave train pattern over the east Pacific and North America and induces a low (high) off the west coast and a high (low) over North America in the La Niña (El Niño) case (Figs. 9c,d).

The eddy forcing over only the Eastern Hemisphere (Figs. 10a,b) excites a wave train arching from South Asia to North America, which has the same spatial structure and the opposite polarity in the El Niño and La Niña simulations. The forcing over only the Western Hemisphere (Figs. 10c,d) generates stronger responses over the east Pacific and North America, and the El Niño pattern is nearly in quadrature with the La Niña pattern.

The response to the tropical eddy forcing (0°–30°N) is compared to the response to the midlatitude eddy forcing (30°–60°N) in Figs. 10e–h. Interestingly, the responses to the eddy forcings in these two regions tend to cancel out each other in many areas. Over North America, they generate responses of different structures. The tropical eddy forcing in the El Niño simulation excites a high centered over Canada that extends southward to the United States, and the midlatitude eddy forcing induces a high in the south and a low in the north. In the La Niña case, the tropical eddy forcing generates a high over the central United States and a low along the East Coast. The response to the midlatitude eddy forcing has a north–south tripole pattern, with a high in the middle at 30°–50°N. Therefore, the tropical and extratropical eddy forcings both contribute to the anomalous patterns over North America in the El Niño and La Niña simulations.

5. Conclusions

Composites of the NCEP–NCAR reanalysis data show that the La Niña pattern is dominated by a strong high over North America while the El Niño pattern has a weak high that is below the 95% confidence level. This implies a weak linear correlation between the Niño-3 SSTAs and North American circulation anomalies. Composite analyses of precipitation and surface air temperature over North America also reveal different patterns for El Niño and La Niña. The surface air temperature response to La Niña is stronger and more coherent.

A linear barotropic model is used to diagnose the mechanisms involved in the maintenance of the anomaly patterns. Various forcing terms derived from a one-level vorticity budget analysis based on observations are used to force the model. When all forcing terms are included, the model responses are similar to the observed patterns, and a strong and extensive anticyclone is reproduced in the La Niña simulation. Two terms contribute most to the responses over North America: the stretching term and the transient eddy term. The stretching term generates a cyclone over North America in the El Niño simulation and an anticyclone in the La Niña simulation, and the La Niña

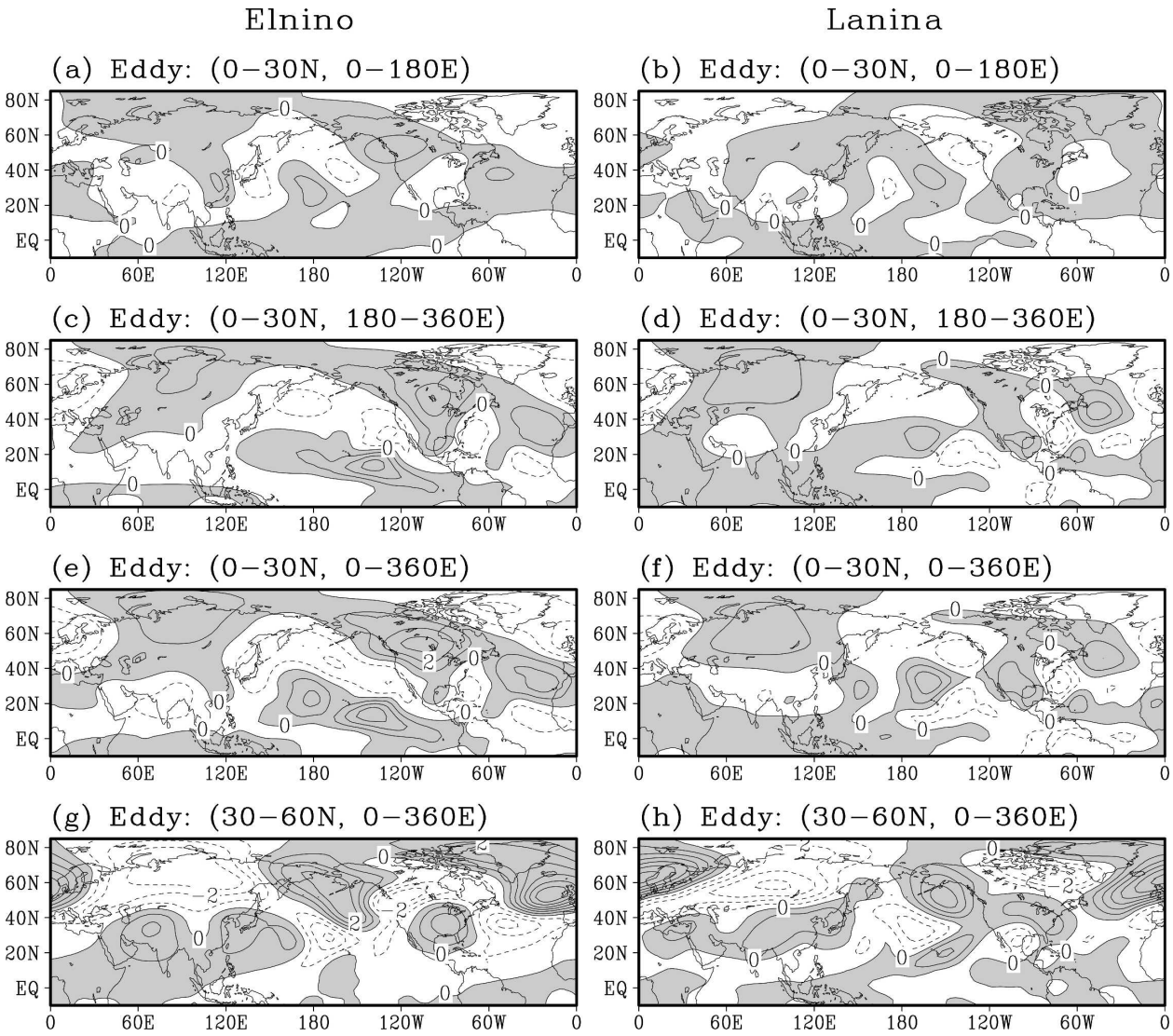

FIG. 10. Same as Fig. 9, but for the eddy forcing term over different regions.

anticyclone is slightly stronger. However, the transient eddy forcing generates an anticyclone over North America in both El Niño and La Niña simulations, which weakens the El Niño response and enhances the La Niña response.

The perplexing part of the results is the strong asymmetry of the barotropic model response to the transient eddy forcing. It is not clear why the transient eddy feedback is insensitive to the polarity of the eastern Pacific SST anomalies. Some previous studies have examined the role of nonlinearity using baroclinic models (e.g., Jin and Hoskins 1995; Ting and Yu 1998). In most baroclinic simulations, extratropical transient eddies were suppressed by strong damping or diffusion, or the time integration was terminated before baroclinic instability and transient eddies develop. Therefore, the interaction between the low-frequency flow and transient eddies was very weak in these models, and the nonlinearity arises mainly from the wave–wave interactions and interactions between the thermal forcing and topographic forcing. Some AGCM simulations (Palmer and Sun 1985; Pitcher et al. 1988; Kushnir and Lau 1992) found that warm and cold SSTAs generate extratropical responses of the same polarity. Diagnoses of these AGCM simulations suggested that transient eddies play a key role in sustaining the extratropical responses despite the opposite polarity of SSTAs. Although the transient eddies may be unrealistically vigorous in these AGCMs, these studies suggest the nonlinear nature of the transient eddy processes and their importance in maintaining the extratropical response. Also of note is that the barotropic model responses to the stretching

term (*fD*) in the El Niño and La Niña simulations have different structures over the North Pacific and North America. It is not clear how sensitive the transient eddy feedback is to the changes in low-frequency patterns.

Acknowledgments. This work was supported by the NOAA Pan American Climate Studies Program and the NSF Climate Dynamics Program under Grant ATM03-29531 at the University of Hawaii at Manoa, and by NOAA under Grant NA01AANRG0011 and NSF under Grant ATM-0101135 at the Naval Postgraduate School.

REFERENCES

Adams, D. K., and A. C. Comrie, 1997: The North American monsoon. *Bull. Amer. Meteor. Soc.,* **78,** 2197–2213.

DeWeaver, E., and S. Nigam, 2002: Linearity in ENSO's atmospheric response. *J. Climate,* **15,** 2446–2461.

Geisler, J. E., M. L. Blackmon, G. T. Bates, and S. Muñoz, 1985: Sensitivity of January climate response to the magnitude and position of equatorial Pacific sea surface temperature anomalies. *J. Atmos. Sci.,* **42,** 1037–1049.

Gershunov, A., and T. P. Barnett, 1998: Interdecadal modulation of ENSO teleconnections. *Bull. Amer. Meteor. Soc.,* **79,** 2715–2725.

Gill, A. E., 1980: Some simple solutions for heat-induced tropical circulation. *Quart. J. Roy. Meteor. Soc.,* **106,** 447–462.

Hall, N. M. J., and J. Derome, 2000: Transience, nonlinearity, and eddy feedback in the remote response to El Niño. *J. Atmos. Sci.,* **57,** 3992–4007.

Halpert, M. S., and C. F. Ropelewski, 1992: Surface temperature patterns associated with the Southern Oscillation. *J. Climate,* **5,** 577–593.

Held, I. M., S. W. Lyons, and S. Nigam, 1989: Transients and the extratropical response to El Niño. *J. Atmos. Sci.,* **46,** 163–176.

——, M. Ting, and H. Wang, 2002: Northern winter stationary waves: Theory and modeling. *J. Climate,* **15,** 2125–2144.

Hoerling, M. P., and M. Ting, 1994: Organization of extratropical transients during El Niño. *J. Climate,* **7,** 745–766.

——, A. Kumar, and M. Zhong, 1997: El Niño, La Niña, and the nonlinearity of their teleconnections. *J. Climate,* **10,** 1769–1786.

——, ——, and T. Xu, 2001: Robustness of the nonlinear climate response to ENSO's extreme phases. *J. Climate,* **14,** 1277–1293.

Hu, Q., 2003: A multidecadal variation in summer season diurnal rainfall in the central United States. *J. Climate,* **16,** 174–178.

——, and S. Feng, 2001: Variations of teleconnection of ENSO and interannual variation in summer rainfall in the central United States. *J. Climate,* **14,** 2469–2480.

Jin, F.-F., and B. J. Hoskins, 1995: The direct response to tropical heating in a baroclinic atmosphere. *J. Atmos. Sci.,* **52,** 307–319.

Kalnay, E., and Coauthors, 1996: The NCEP/NCAR 40-Year Reanalysis Project. *Bull. Amer. Meteor. Soc.,* **77,** 437–471.

Kang, I.-S., and I. M. Held, 1986: Linear and nonlinear diagnostic models of stationary eddies in the upper troposphere during northern summer. *J. Atmos. Sci.,* **43,** 3045–3057.

Kushnir, Y., and N.-C. Lau, 1992: The general circulation model response to a North Pacific SST anomaly: Dependence on time scale and pattern polarity. *J. Climate,* **5,** 271–283.

Matsuno, T., 1966: Quasi-geostrophic motions in the equatorial area. *J. Meteor. Soc. Japan,* **44,** 25–43.

Mo, K. C., J. N. Paegle, and R. W. Higgins, 1997: Atmospheric processes associated with summer floods and droughts in the central United States. *J. Climate,* **10,** 3028–3046.

Montroy, D. L., M. B. Richman, and P. J. Lamb, 1998: Observed nonlinearities of monthly teleconnections between tropical Pacific sea surface temperature anomalies and central and eastern North American precipitation. *J. Climate,* **11,** 1812–1835.

Namias, J., 1991: Spring and summer 1988 drought over the contiguous United States—Causes and prediction. *J. Climate,* **4,** 54–65.

Palmer, T. N., and Z. Sun, 1985: A modelling and observational study of the relationship between sea surface temperature in the north-west Atlantic and atmospheric general circulation. *Quart. J. Roy. Meteor. Soc.,* **111,** 947–975.

Pitcher, E. J., M. L. Blackmon, G. T. Bates, and S. Muñoz, 1988: The effect of North Pacific sea surface temperature anomalies on the January climate of a general circulation model. *J. Atmos. Sci.,* **45,** 173–188.

Ropelewski, C. F., and M. S. Halpert, 1986: North American precipitation and temperature patterns associated with the El Niño/Southern Oscillation (ENSO). *Mon. Wea. Rev.,* **114,** 2352–2362.

Sardeshmukh, P. D., G. P. Compo, and C. Penland, 2000: Changes of probability associated with El Niño. *J. Climate,* **13,** 4268–4286.

Smith, T. M., and R. W. Reynolds, 2004: Improved extended reconstruction of SST (1854–1997). *J. Climate,* **17,** 2466–2477.

Ting, M., and H. Wang, 1997: Summertime U.S. precipitation variability and its relation to Pacific sea surface temperature. *J. Climate,* **10,** 1853–1873.

——, and L. Yu, 1998: Steady response to tropical heating in wavy linear and nonlinear baroclinic models. *J. Atmos. Sci.,* **55,** 3565–3582.

——, M. P. Hoerling, T. Xu, and A. Kumar, 1996: Northern Hemisphere teleconnection patterns during extreme phases of the zonal-mean circulation. *J. Climate,* **9,** 2614–2633.

——, H. Wang, and L. Yu, 2001: Nonlinear stationary wave maintenance and seasonal cycle in the GFDL R30 GCM. *J. Atmos. Sci.,* **58,** 2331–2354.

Trenberth, K. E., 1997: The definition of El Niño. *Bull. Amer. Meteor. Soc.,* **78,** 2771–2777.

——, and G. W. Branstator, 1992: Issues in establishing causes of the 1988 drought over North America. *J. Climate,* **5,** 159–172.

——, and C. J. Guillemot, 1996: Physical processes involved in the 1988 drought and 1993 floods in North America. *J. Climate,* **9,** 1288–1298.

——, G. Branstator, and P. A. Arkin, 1988: Origins of the 1988 North American drought. *Science,* **242,** 1640–1645.

Wang, Z., C.-P. Chang, B. Wang, and F.-F. Jin, 2005: Teleconnections from Tropics to northern extratropics through a southerly conveyor. *J. Atmos. Sci.,* **62,** 4057–4070.

Webster, P. J., and T. N. Palmer, 1997: The past and the future of El Niño. *Nature,* **390,** 562–564.

Wu, A., and W. W. Hsieh, 2004: The nonlinear Northern Hemisphere winter atmospheric response to ENSO. *Geophys. Res. Lett.,* **31,** L02203, doi:10.1029/2003GL018885.